Design Optimization of Pixel Structure for α-Si based Uncooled Infrared Detector

Sudha Gupta*, Anupriya Katiyar, R.K. Bhan, and R. Muralidharan

Solid State Physics Laboratory, Delhi – 110 054, India
E-mail: sudha@sspl.drdo.in

ABSTRACT

In this paper authors present the design and simulation results achieved for pixel structure of amorphous Si (α-Si) based bolometer array. Most uncooled IR detectors in the world are based on VOx material. But this is not a standard material in IC technology and has many inherent disadvantages. The α-Si, an alternative material with high TCR is becoming as popular. However, large TCR values, in this material are achieved only in films of high resistivity. To achieve TCR value more than 2.5%/K, α-Si film resistivity is ~ 80 ohms-cm. This gives rise to very large pixel resistance of the order of 100 Mega ohms depending upon the design of the leg structure. This high pixel resistance causes very large noise and hence lower sensitivity. If leg width or membrane thickness is increased in order to reduce the pixel resistance, then this results in higher thermal conductance which also decreases sensitivity. To overcome this problem, pixel structure is so designed that within a pixel, only part of the electrical conduction is through α-Si and rest is through metal. Simulation using Coventorware software has been done to optimize pixel resistance as well as thermal conductance through legs so that maximum sensitivity could be obtained. Optimization is also carried out in order to reduce sensitivity of pixel resistance to variation in material resistivity.

Keywords: Uncooled infrared detector, microbolometer, thermal conductance

1. INTRODUCTION

Infrared focal plane array (IRFPA) that forms the heart of a thermal camera consists mainly of two devices:
(a) An IR sensor or detector array and
(b) A readout integrated circuit (ROIC) array.

An infrared (IR) detector senses the incoming IR radiation and converts the optical signal into the electrical signal while ROIC array processes and amplifies that electrical signal from the sensor array which is finally fed to the output video amplifier to produce image. IR detectors are basically of two types: cooled (based on photon detection) or uncooled (based on thermal detection). In photon detectors, incident IR power causes generation of charge carriers in the detector material which help in the detection process. However, for detection of IR wavelengths in the 8-14 micrometer range, photon detectors must be cooled to cryogenic temperatures to minimize thermally induced carriers. These detectors have very high quantum efficiency and very low noise equivalent temperature difference (NETD), but the material technology is often quite difficult. Further, requirement of cooling to cryogenic temperature results in increase of cost, power consumption, weight and size of the imaging system and also causes reliability problems. Uncooled infrared detectors, though less sensitive than cooled detectors, have become an excellent alternative to the cooled detectors and are commonly used in many commercial, industrial and military IR camera products.

In thermal detectors the incident radiation induces a change in temperature of the detector that causes a change in some physical characteristic of the detector element, be it mechanical, electrical, optical or otherwise. Since thermally generated electron-hole pairs do not interfere in the detection process, the impact of thermal noise is more controllable and room temperature operation of a thermal detector is possible. Microbolometer technology, at present, is leading among uncooled thermal sensors. The development of microbolometer based focal plane arrays, which rely on the temperature coefficient of resistance to sense temperature excursions, have enabled high-resolution thermal images to be obtained at room temperature. This significant advance brought infrared and long-wave imaging to a wide-range of applications for which cryogenic cooling requirements had earlier limited their utility. Without a cooling circuit in the system, uncooled IR thermal detectors are more rugged, less bulky, lightweight, easy to maintain and use less power than cooled detectors. Additionally, they can offer a wide spectral response The variable output of a light-sensitive device that is based on the color of the light it perceives. and longer periods of operation than the cooled photon detector.

As uncooled technology moved forward, vanadium oxide (VOx) was seen as the detector material of choice. This material is not a standard material in IC fabrication and hence increases cost of manufacturing. Secondly, since it is not a single material, compositional variation has to be controlled very precisely. This is very important as any composition variation will compromise uniformity which is a very important parameter for imaging. Amorphous silicon, a high TCR material has emerged as an alternative material. α-Si microbolometers developed using MEMS technology have all the advantages

of silicon processing including cost and yield. Another benefit is high spatial uniformity as the composition of amorphous silicon presents negligible variations. A VOx microbolometer membrane is thicker than that of α-Si which is a disadvantage for detection at high frequency signal. Being inherently stiff, α-Si permits the construction of smaller bridging structures in the array. The smaller the bridge structure, the smaller the pixel and, therefore more elements can be built into a given array size. This bridging structure is also shorter and, thus, more resistant to vibration. α-Si microbolometers exhibit higher effective thermal insulation compared with VOx based devices due to thinner membranes. Another advantage of α-Si based bolometer is its predictable temperature behavior, a factor that contributes to easier sensor operation in changing ambient temperatures and its usefulness in low-power-consumption focal-plane arrays that save batteries when used in applications like handheld cameras. Thermal time constant ~ 30% to 40% lower than vanadium oxide sensors can be achieved in amorphous silicon (10 ms) thus enabling the design of faster sensors. However, the main disadvantage in using α-Si as detector material is its high resistance which gives rise to high noise and hence lower sensitivity.

In this paper we present the design and simulation results achieved for different structures of α-Si based bolometer pixel. A microbolometer pixel is composed of a thermometer integrated on a micro-bridge. This micro-bridge is supported by two legs anchored over the silicon substrate by metal studs, as shown in Fig.1. This micro-bridge is built on a sacrificial layer which is removed in a final step. The vacuum gap thus created works as a quarter wavelength cavity, which sets the detector spectral response maximum at a wavelength close to 10 µm. The incident IR radiation is absorbed and raises the temperature of the bolometer material. The output signal (voltage or current) is observed as a change in resistance due to the rise in its temperature. So for high sensitivity, the detector material needs to have a high temperature coefficient of resistance, i.e., its resistance should be a sensitive function of temperature. At the same time, the support structure is required to be designed to have excellent thermal isolation, that is, a very small value of thermal conductance, G and low noise to be able to extract a very low signal. To achieve good performance, a proper design is required to develop a microbolometer.

The micro-bridge consists of various layers. Si_3N_4 is used as support layer as well as for passivation. α-Si is the detector material which is sandwiched between two thin Si_3N_4 layers. A thin TiN layer with vacuum impedance matching is grown at the top so that due to quarter wave cavity below the membrane, almost entire IR radiation is absorbed within the membrane. This layer is also called absorber layer.

2. THEORY

Performance of a bolometer pixel depends upon a number of material and design parameters. Certain figures of merit such as temperature coefficient of resistance (TCR), responsivity (R_v) and detectivity (D*) have been defined to indicate the performance. The NETD and D* are figures of merit for sensitivity and thermal time constant shows how fast a detector responds. The responsivity R_v of an IR pixel is defined as the output signal (voltage or current) divided by the input radiant power falling on the pixel.

The analysis of thermal IR detectors begins by solving the heat flow equation that describes the temperature increase in terms of the incident radiant power following Wood's[1]. If the incident power varies sinusoidally with frequency ω, then the heat flow equation describing the pixel is:

$$C \frac{d(\Delta T)}{dt} + G(\Delta T) = \eta P_0 \exp(j\omega t) \qquad (1)$$

where,

C - Heat capacity of the micro-bridge
G - Thermal conductance
Po- Amplitudes of modulated IR radiation power falling on pixel
η - Absorptivity of IR sensitive films
ΔT - Temperature increase of the sensitive area of the pixel
t - Time

This simplified equation assumes that the power dissipation in the sensitive area due to applied electrical bias can be neglected.

The solution of equation (1) is

$$\Delta T = \frac{\eta P_O \exp(j\omega t)}{G + j\omega C} = \frac{\eta P_O}{G\left(1 + \omega^2 \tau^2\right)^{1/2}} \qquad (2)$$

where τ is the thermal response time defined as

$$\tau = C/G \qquad (3)$$

For α-Si, the resistance varies with temperature as

$$R(T) = R_0 \exp(\Delta E/kT) \qquad (4)$$

where ΔE is the activation energy, equal to half the bandgap E_g, and R_0 is a constant. Temperature coefficient of resistance, TCR, of a-Si is given by
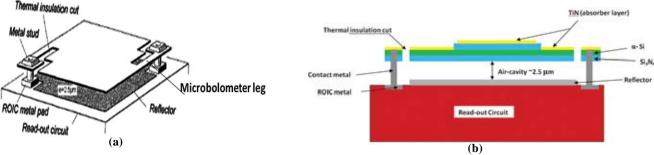

(a)

(b)

Figure 1. Structure of microbolometer pixel (a) top view taken[7] and (b) cross-sectional view showing different layers of microbolometer membrane

$$\alpha = \frac{1}{R}\frac{dR}{dT} = -\frac{\Delta E}{kT^2} \tag{5}$$

Let the output signal be the current I_s, then

$$I_S = V_b \Delta R / R^2 = V_b \alpha \Delta T / R \tag{6}$$

where V_b is the bias voltage across the pixel. The temperature increase ΔT is given by Eqn (2). Thus the signal current is

$$I_S = V_b \frac{\alpha \eta P_0}{[RG(1+\omega^2\tau^2)^{\frac{1}{2}}]} \tag{7}$$

So that current responsivity (R_I) is given by

$$R_I = \frac{I_S}{P_0} \tag{8}$$

Voltage responsivity, $R_V = R_I \times R$ is given by

$$R_V = V_b \frac{\alpha \eta}{G(1+\omega^2\tau^2)^{\frac{1}{2}}} \tag{9}$$

Equation (8) shows that the responsivity is directly proportional to α and inversely proportional to the thermal conductance (G) associated with the heat loss mechanisms. We denote thermal conductance of support structure (legs) of the pixel by G_{leg}. Maximum heat conduction takes place through G_{leg} which depends upon leg dimensions and leg material. If g_{leg} is the conductivity of leg material and A and L are respectively its area and length, then G_{leg} is given by

$$G_{leg} = g_{leg} A/L \tag{10}$$

From Fig. 1(b), it is evident that all layers of the membrane will contribute to heat loss as they provide parallel paths for heat conduction. Thermal conduction of each membrane layer in the leg is, thus, added to obtain the value of G_{leg}. Dependence of G_{leg} on leg length is plotted in Fig. 2 There are other sources of heat losses as well. For small changes in microbolometer temperature dT, the corresponding increments in the radiation power emitted from the microbolometer $P_{rad} = (2A)\varepsilon\sigma T^4$ can be written in terms of radiation thermal conductance (G_{rad}):

$$G_{rad} = \frac{d}{dT}(2A\varepsilon\sigma T^4) = 4(2A\varepsilon\sigma T^3)W/K \tag{11}$$

Heat loss due to convection or conduction by air can be made very small by mounting sensor array in an evacuated package. There is another source of thermal conductance, G_e arising due to bias heating. For fixed bias voltage across the detector, bias heating may be written as $W_h = V^2/R$, where R is the bolometer pixel resistance. This may be rewritten as $G_e.\Delta T = dW_h/dT.\Delta T = -V^2/R.\alpha.\Delta T$. Conductance G_e arises due to electrothermal feedback and is negative for constant voltage biasing. So total conductance.

$$G = G_{leg} + G_{rad} - G_e \tag{12}$$

May even become zero since TCR is –ve for α-Si. This may give rise to thermal runaway situation for very low values of G_{leg} or high voltage values. Variation of G with leg conductance is shown in Fig.3. Thermal runaway region is also shown. This region has to be avoided while designing α-Si bolometer.

Equation (2) is basic to thermal IR arrays. It describes the temperature increase of the resistive area of the pixel when radiation of power amplitude Po sinusoidally modulated with angular frequency ω falls on the sensitive area. The pixel temperature increases and decreases as the input radiant power rises and falls in an oscillatory manner. The transition between the low and high frequency regions is characterized by the thermal time constant, τ.

Another important parameter of thermal IR detector is, detectivity and is given by

$$D^* = (Rv \sqrt{A\Delta f})/Vn \tag{13}$$

where Δf is the detector noise bandwidth (Hz), Vn is the total detector noise (V) and A is the detector area. The other important measure of the performance of IR imaging system is NETD that is the difference in the temperatures of objects in a scene, which will produce a signal to noise ratio of one. It is given by

$$NETD = \frac{4F^2 V_n}{\tau_O A R_V \left(\frac{\Delta P}{\Delta T}\right)_{\lambda_1 - \lambda_2}} \tag{14}$$

where F is the focal ratio of the optics and τ_0, is the transmittance of the optics, $(\Delta P/\Delta T)_{\lambda_1-\lambda_2}$ is the change in power per unit area radiated by scene (or black body) at temperature T, with respect to T measured within the spectral band from λ_1 to λ_2.

3. NOISE OF A BOLOMETER PIXEL

Most dominant sources of noise in a-Si based bolometer are:

(a) 1/f Noise: This noise is very important for α-Si based detectors and is very much process dependent. It is modeled as :

$$V_{\frac{1}{f}} = V_b \sqrt{K_{1/f} \ln\left(\frac{1}{2t_I f_1}\right)} \tag{15}$$

where $K_{1/f}$ is the 1/f noise constant and t_1 is the integration time. Upper frequency limit, f_2 is taken as $1/2t_1$. Bandwidth is $f_2 - f_1$

(b) Johnson Noise: Since pixel resistance is large in this case, a significant Johnson noise is also present in α-Si bolometer pixels. This noise is given by:

$$V_J = \sqrt{4KTR\left(\frac{1}{2t_I} - f_1\right)} \tag{16}$$

(c) Temperature Noise: This noise is generally much smaller than 1/f noise and Johnson noise. It is given by

$$V_{temp} = \propto V_b \sqrt{\frac{KT^2}{C}} \tag{17}$$

Total noise of the detector is obtained by adding individual noise terms in quadrature:

$$V_n = \sqrt{V_{1/f}^2 + V_J^2 + V_{temp}^2} \tag{18}$$

4. MODELLING AND SIMULATION

In this work, we present the design and simulation results achieved for pixel structure of Amorphous Si (α-Si) based bolometer array. NETD is the fundamental performance parameter of a thermal imaging array. Lower the value of

NETD, more sensitive is the detector. Another important parameter is its speed that depends upon thermal time constant, τ. If scene is changing rapidly, then high speed detectors, and hence low value of τ is required. Another important factor is uniformity of response of different pixels in an array which is achieved by lower sensitivity of NETD and τ to material properties.

Equations (8) to (17) show that to achieve low NETD, detector's responsivity should be large and it should have low noise. Further, large responsivity value may be obtained by chosing detector material of large TCR value and high absorptivity for IR radiation. Also the pixel should be designed to have low thermal conductance, G and high fill factor. On the other hand, for faster detectors, $\tau = C/G$ should also be small. Thus thin membranes with low thermal mass and low G should be designed to achieve high sensitivity as well as speed. In fact, G is the most important factor that effects both sensitivity and speed of the detector. Moreover, its value may vary over a very large range depending upon design parameters. A thin TiN layer at the top is deposited for impedance matching with vacuum which along with quarter wave cavity enables to achieve absorptivity of more than 80% in the entire 8-14 μm region of the incident IR radiation[2]. Most important noise sources in semiconductor bolometer detectors are 1/f noise and Johnson noise. Both of these noise values are high for large resistance values of the pixel. It is found experimentally in α-Si films that high TCR values are achieved on high resistivity films[3]. In addition, assuming contact resistance ~ 0.1 Mohms in each contact means 0.2 MΩ of total contact resistance is added to the pixel resistance. NETD and thermal time constant that can be achieved for different pixel designs has been simulated for enabling one to determine the suitable design parameters. Table 1 shows values of various parameters used in the calculations.

5. DESIGN OPTIMIZATION

A microbolometer pixel absorbs incident IR radiation, thereby increasing its temperature. The change in its resistance value is the measure of IR radiation absorbed by it. Thus, to maximize its sensitivity, it is important to reduce the loss of heat from the pixel. Maximum heat loss from the pixel occurs due to conduction through its legs which is governed by G_{leg}. Equation (10) shows that G_{leg} depends upon leg length, leg width and thermal conductivity and thickness of the constituent layers of the membrane. As thermal conductivity of various layers is constant, thus, leg structure is the most important parameter in design of bolometer pixel that controls pixel sensitivity. Minimum value of leg width is guided by process capability and large value is detrimental to high sensitivity, so leg width can not be varied too much. The requirement that maximum IR radiation has to be absorbed in the membrane in order to increase its temperature and large thickness is undesirable to obtain high speed (low value of τ), so thickness of various layers is also almost fixed. In present calculations, leg width is taken as 2 μm and thickness of various layers is taken as given in Table 1. The parameter that can be varied is leg length. Figure 2 shows dependence of leg thermal conductance and thermal time constant on leg length. It can be seen that as the leg length increases, G_{leg} decreases. This is expected as increase in leg length implies that the distance between the membrane and contact metal is increased. Thus thermal gradient is created over a larger length. Low thermal conductance is essential for achieving high sensitivity of the pixel. However, thermal time constant increases due to decrease of G_{leg}. Thus, some compromise has to be made depending upon desired value of sensitivity and speed of the detector. Thermal time constant may also be reduced by reducing membrane's thermal mass. However, it should be thick enough to be resistant to vibrations depending upon the desired application.

Table 1. Parameter values used in the calculations

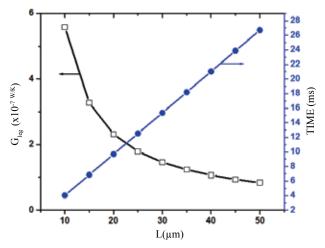| Parameter	Value
Pitch	45 μm x 45 μm
TCR	-0.025
DL/dT (W/cm^2/K)	8.4E-5π
Emissivity of the target	0.9
Absorptivity (membrane)	0.8
Transmission (optics)	0.9
Vbias	3 v
$K_{1/f}$	10^{-11}
F# of optics	1
Leg width	20 μm
Thickness of membrane layers	
α-Si	200 nm
Si_3N_4	200 nm
TiN	10 nm
Contact metal (Al)	600 nm

Figure 2. Variation of thermal conductance of leg and thermal time constant as a function of leg length (L).

The parameter that is used in evaluation of NETD (Eqn. (14)) is thermal conductance (G). G can be calculated from Eqn. (12). It depends mainly upon G_{leg}, but also has significant dependence on R, the pixel resistance specially for low values of R. Variation of G with variation in G_{leg} and R is plotted in Fig. 3. For all values of R, G increases linearly with G_{leg}. However, G becomes negative in the region where both pixel resistance, R and G_{leg} have low values. This is the thermal runaway region which needs to be avoided for stable operation of the thermal
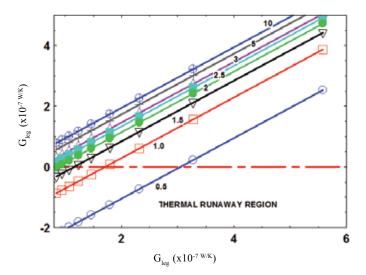
Figure 3. Dependence of total thermal conductance of the pixel on thermal conductance of the legs. Pixel resistance values in Mohms are indicated on each curve.

Figure 4. NETD values that can be achieved for leg length (L) and pixel resistance (R). Leg thermal conductance corresponding to each L value is indicated on the top x-axis. R values, as indicated on each curve, are in Mohms.

detector. While G_{leg} depends upon leg geometry and thermal conductivity of leg material layers; R depends upon membrane geometry and electrical resistivity of the membrane layers. For a particular resistance value, G is negative for very low values of G_{leg} or large values of leg length. As leg length is decreased, G_{leg} increases and G also increases. At a particular value it becomes zero. Let the value of leg length and leg thermal conductace where G becomes zero be denoted by L_0 and G_{leg0} respectively. As the resistance value is increased, L_0 increases and G_{leg0} decreases. Thus, a suitable combination of leg length and pixel resistance should be chosen to obtain desired value of thermal conductance.

Figure 4 has been plotted by evaluating NETD values using Eqns. (8), (11), and (15). Curves show dependence of NETD as function of leg length, L and pixel resistance, R. Thermal conductance of legs, G_{leg} is also shown at the top x-axis in the figure. For a particular R value, NETD decreases as the leg length increases. This is due to decrease in G_{leg} and hence increase in responsivity. However, when L becomes equal to L_0, NETD is zero and it becomes negative if L is increased further. This is the region where bolometer operation is unstable. Thus, leg length should always be smaller than L_0. As R is increased, L_0 becomes larger and there is little chance of NETD becoming zero or negative. For a given leg length, NETD increases as R increases. In Fig. 4, a dashed line is drawn at NETD = 80 mK. If a microbolometer pixel is required to give NETD less than 80 mK, then leg length and resistance value of the pixel should be such be such that it lies between the two lines drawn at NETD equal to zero and NETD = 80 mK.

An α-Si film of resistivity 80 Ω-cm gives rise to pixel (Fig. 5(a)) resistance of ~62 MΩ for leg length 15 µm and ~126 MΩ for leg length of 30 µm. It is clear from Fig. 4 that low NETD values cannot be achieved with such high resistance values. Thus, it is essential to either provide parallel current paths or current is allowed to flow partially through low resistive material in the membrane. Most of the pixel resistance contribution
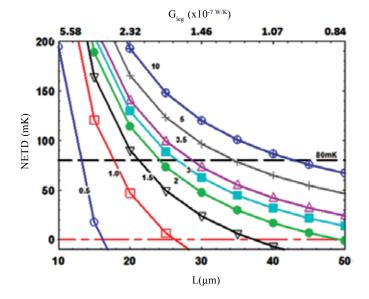
is from the leg structure. Thus, current in the leg structure is generally made to flow through metal. Design should ensure that thermal conductance does not increase by this, otherwise NETD value will again rise. This has been achieved in modified pixel structure of Fig. 5(b) by shorting absorber TiN layer with α-Si in the leg region (see Fig. 1(b)) and partially in the membrane region so as to obtain pixel resistance ~2 MΩ for film resistivity of 80 MΩ. Grid-type and serpentine pixel membrane structures have been presented by Michel Vilain and Saint Georges de Commiers in patents[4-6]. These are shown in Figs. 5(c) and 5(d). To compare various pixel structures, we simulated pixel resistance as well as thermal conductance of all structures in Figs. 5(a) to 5(d). We have used Coventorware software for these simulations. Table 2 shows the results for different values of leg length. Film thicknesses and leg width are kept fixed for all the structures for comparison. For comparing different structures, let NETD < 80 mK is required for some application. A dashed line showing NETD = 80 mK is plotted in Fig. 4. Now an IR detector with resistance and thermal conductance values within the two dashed lines y = 0 and y = 80 mK is suitable for our purpose. 5th column in Table 2 is marked as 'Yes' or 'No' depending upon whether the pixel is suitable or not for the application. It can be noted that structures of Figs. 5(c) and 5(d) give NETD < 80 mK for L more than 20 µm and structure Fig. 5(d) gives low value of NETD for shortest values of L. Achieving high sensitivity at short leg lengths allows one to obtain more stable pixel as stress in the membrane is reduced. However, there is one flaw in the calculations. We have assumed same value of 1/f noise constant for all the structures. It is generally known that this parameter depends upon the α-Si material volume that is taking part in electrical conduction. Larger this volume, lesser is the 1/f noise. Since same thickness has been considered in all the structures, thus one with largest area will have the
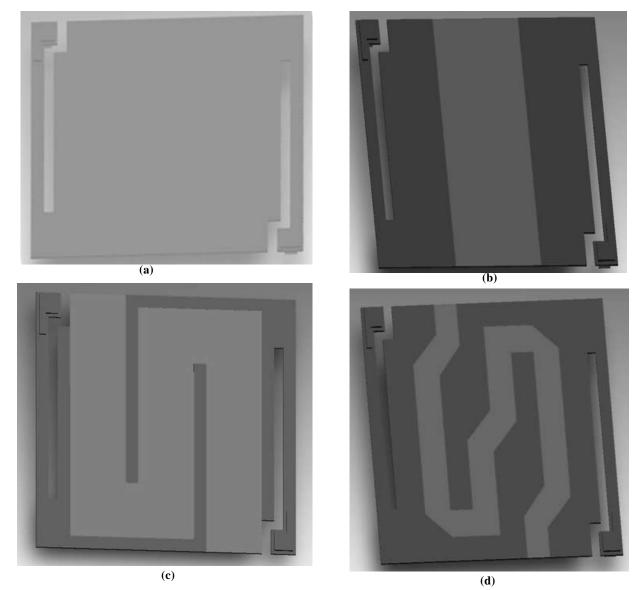
(a)

(b)

(c)

(d)

Figure 5. (a) conventional structure (b) modified structure (c) grid structure (d) serpentine structure, are different pixel membrane structures considered in this work. Dark areas show regions where electrical conduction occurs through TiN while in light regions current flows through α-Si.

least noise. Column 6 of Table 2 shows the area of α-Si that is participating in electrical conduction. Grid structure of Fig. 5(c) has almost double the area as compared to serpentine structure of Fig. 5(d).

Yet another important issue in an IR detector array is sensitivity of pixel resistance to variation in α-Si film resistivity. Figure 6 shows pixel resistance variation with α-Si film resistivity for pixel structures of Figs. 5(b) to 5(d). It can be seen that pixel structure of Fig. 5(b) is most sensitive to variation in film resistivity. Hence, this structure can be used for imaging arrays only if it is possible to deposit α-Si films with very high uniformity in resistivity value.

6. CONCLUSION

Our analysis shows that pixel membrane structures of grid type and serpentine type (Figs. 5(c) and 5(d) respectively) are more appropriate for achieving high performance thermal imaging arrays. Leg dimensions need to be chosen depending
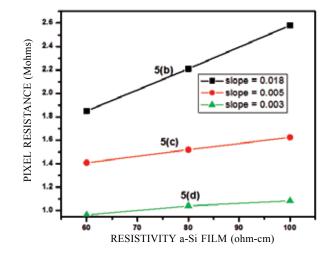

Figure 6. Pixel resistance variation with α-Si film resistivity for pixel structures of Figs 5(b) to 5(d).

586

Table 2. Simulated values of parameters for pixel structures in Figures 5(a) - 5(d) for different leg lengths

Structure	Leg length (µm)	Resistance (MΩ) (Resistivity A_Si 80 Ω-cm)	Thermal conductance (x10⁻⁷ W/K)	Suitability for NETD < 80 mK	Area A_Si (µm²)
Conventional structure (Fig. 5(a))	15	62.74	2.68	No	1679
	20	83.25	2.02	No	1664
	25	104.35	1.634	No	1649
	30	126.58	1.35	No	1634
	35	152.38	1.12	No	1619
Modified structure (Fig. 5(b))	15	1.90	2.66	No	630
	20	2.05	2.014	No	630
	25	2.21	1.616	Yes	630
	30	2.38	1.344	Yes	630
	35	2.59	1.12	Yes	630
Grid structure (Fig. 5(c))	15	1.254	2.646	No	1062
	20	1.378	2.0	No	1062
	25	1.519	1.608	Yes	1062
	30	1.668	1.337	Yes	1062
	35	1.84	1.116	Yes	1062
Serpentine structure (Fig. 5(d))	15	0.73	2.66	No	550
	20	0.899	2.01	Yes	550
	25	1.04	1.61	Yes	550
	30	1.19	1.34	Yes	550
	35	1.36	1.139	Yes	550

upon required values of NETD and τ and process capabilities. If deposition of α-Si film is controlled enough to give low 1/f noise such that this component is not dominating, then serpentine structure of Fig. 5(d) gives best NETD values. Otherwise grid structure of Fig. 5(c) may be more suitable as this structure has more area of α-Si that is participating in electrical conduction. So lower 1/f noise is expected in this structure.

REFERENCES

1. Wood, R.A. Monolithic silicon microbolometer arrays. *In* Semiconductors and Semimetals, 47, pp. 44-121, Academic Press, San Diego, USA, 1997.
2. Toy, M. Fatih. Uncooled infrared thermo-mechanical detector array: Design, fabrication and testing. *Sensors and Actuators A*, 2009, **156**, 88–94.
3. Mottin, E. Uncooled amorphous silicon technology enhancement for 25 µm pixel pitch achievement. Infrared Technology and Applications XXVIII, SPIE, 2002, **4820**.
4. Vilain, Michel & Georges, Saint de Commiers (FR). Bolometric detector, infrared detection device employing such a bolometric detector and process for fabricating this detector. Patent No. US 007138630B2, 21Nov., 2006.
5. Vilain, Michel & Georges, Saint de Commiers (FR), TBolometric detector, infrared detection device employing such a bolometric detector and process for fabricating this detector. Patent No. US 20050082481A1, 21 April, 2005.
6. Vilain, Michel & Georges, Saint de Commiers (FR), Device for detecting infrared radiation with bolometric detectors. Patent No. US 007288765 B2, 30 Oct.,2007.
7. Tissot, J.L. Uncooled microbolometer detectors: recent developments at ULIS. *Opto-Electronics Review*, 2006, **14**(1), 25–32.

CONTRIBUTORS

Ms Sudha Gupta received her MSc (Physics) from the University of Delhi, Delhi, in 1986. She joined Solid State Physics Laboratory, Delhi, in 1987 and worked on the development of cooled IR detectors and focal plane arrays. Presently she is working on un-cooled thermal detectors. She has authored or coauthored more than 25 research papers in national and international journals/conferences.

Ms Anupriya Katiyar has completed BTech (Electronics and communication Engg) in 2008 from MMM Engg. College, Gorakhpur. Presently she is working as Scientist 'B' Solid State Physics Laboratory, Delhi. Her research area includes: design of amorphous-Si based microbolometer and photolithography for MEMS based Microbolometer ,RF MEMS switch and microaccelerometer.

Dr R.K. Bhan received his MSc (Physics) from Kashmir University, Srinagar, in 1982 and PhD (Physics) from Delhi University in 1994. Presently he is working as Scientist at Solid State Physics Laboratory, Delhi where he is involved in Infrared Detector characterization and MEMS devices. His research interests include MOS physics, CCDs, IR detectors and FPAs. He has published more than 60 research papers in international journals.

Dr R Muralidharan obtained his MSc (Physics) in 1975 from Madras and PhD from IISc, Bangalore in 1985. Presently working as Director of Solid State Physics Laboratory (SSPL), Delhi. His main area of work is MBE growth and characterisation of epitaxial layers for high electron mobility transistors and quantum dot devices. He is the recipient of -*MRSI Medal 1989, Science Day Award*-2003, and Technology Group Award of DRDO for Advancement in Material Growth using MBE